Turbulent burning velocity of ammonia/oxygen/nitrogen premixed flame in O_2-enriched air condition

Yu Xia[1], Genya Hashimoto[1], Khalid Hadi[1,3], Nozomu Hashimoto[*,1], Akihiro Hayakawa[2], Hideaki Kobayashi[2], Osamu Fujita[1]

[1]Division of Mechanical and Space Engineering, Hokkaido University

Kita13 Nishi8, Kita-ku, Sapporo, Hokkaido 060-8628, Japan

[2]Institute of Fluid Science, Tohoku University

2-1-1 Katahira, Aoba-ku, Sendai, Miyagi 980-8577, Japan

[3]Mechanical Engineering Department,

Politeknik Sultan Azlan Shah, Behrang 35950, Perak, Malaysia

Abstract

Ammonia is a promising hydrogen-energy carrier as well as a carbon-free fuel. However, turbulent burning behavior of ammonia flame had yet to be sufficiently studied. In this work, laminar and turbulent burning velocities of ammonia/oxygen/nitrogen flames were investigated under the condition of oxygen enrichment. The turbulent burning velocity of ammonia/oxygen/nitrogen mixtures was found to increase with increasing turbulence intensity. The ratio of the turbulent burning velocity to stretched laminar burning velocity, U_{tr}/U_N, increased with the turbulence Karlovitz number. However, because of the diffusional–thermal instability effect, given the same turbulent Karlovitz numbers, U_{tr}/U_N in ammonia-lean cases is larger than in ammonia-rich cases. These findings indicate that consideration of the effects of diffusional–thermal instability and of the turbulence is important for the prediction of turbulent flame propagation velocity in ammonia combustion fields.

Keywords: Premixed ammonia/oxygen/nitrogen flame; Turbulent burning velocity; Laminar burning velocity; O_2-enriched combustion

* Corresponding author: Tel.: +81-11-706-6386. E-mail address: nozomu.hashimoto@eng.hokudai.ac.jp

1. Introduction

Given the increasing concerns about environmental impact from power generation by conventional fuels, the search for alternative fuels has become increasingly important. Use of alternative fuels produced from renewable sources can reduce greenhouse gases and pollutant emissions [1]. Ammonia is considered to be one of the most-promising hydrogen-energy-carrier candidates and is an independent alternative to hydrocarbon-based fuels [2]. The combustion of NH_3 does not release CO_2, SO_x and soot [3–5]. Moreover, ammonia can be synthesized from renewable hydrogen and nitrogen separated from air [6]. Since the thermal properties of ammonia are similar to those of propane in terms of boiling temperature and liquefaction pressure, it is economical to be stored in large quantities and transported in liquid-form [7].

However, despite the merits associated with ammonia as a fuel, there are many challenges in ammonia combustion (such as high auto-ignition temperature (903 K), low flammability, high NO_x emission, and low combustion intensity), which make it difficult to use in various energy devices [8,9]. Furthermore, the low combustion intensity of the flame from an ammonia/air mixture makes flame enhancement important for its application as a fuel. Various methods have been proposed to enhance ammonia combustion. Hydrogen addition is a reasonable way of achieving environmentally friendly flame enhancement. The relationship between laminar burning velocity and hydrogen fraction in an ammonia/hydrogen binary fuel was revealed by Ichikawa et al. [10], Lee et al. [5], Li et al. [11] and Kumar et al.[12]. In addition, blending hydrocarbon fuels with ammonia is also important from the perspective of reducing greenhouse-gas emissions. Henshaw et al. [13] and Okafor et al. [14] measured the CH_4/NH_3 mixture laminar burning velocity. Besides, ammonia combustion

under conditions of O_2 enrichment is also a promising way to enhance ammonia combustion due to the thermal enhancement without changing the dominant chemistry. Such O_2-enriched combustion enhances ammonia laminar burning velocity, a positive effect previously verified by Takeishi et al.[15], Li et al. [2] and Mei et al.[16] .

As reviewed above, laminar burning velocity is one of the most important parameters for characterizing ammonia combustion behavior as it contains much physicochemical information. It also is a reference parameter for many premixture flame phenomena, such as extinction, flashback, blow off, and turbulent flame propagation [17]. On the other hand, turbulent flame is also important for the practical use of fuels in combustor. Under turbulent vortices, the flame front is wrinkled, and the flame surface area increases. Turbulence also induces strong, unsteady velocity gradients, which modify the local transport of reactants and lead to local flame structures that depart significantly from the generic one-dimensional flame structures [18]. Thus, a turbulent flame characteristically burns faster than a laminar one. However, because of the weak intensity of premixed ammonia/air flames and corresponding ease of being extinguished, which are due to their low laminar burning velocity [19], most prior ammonia turbulent combustion research focused on the stabilization of ammonia flames [20–23], while no research was conducted to reveal the fundamental turbulent burning behavior of ammonia flame.

Therefore, using a constant-volume spherical chamber, we conducted experiments to study the turbulent burning behavior of ammonia flame under the condition of O_2 enrichment and thus reveal the fundamental turbulent combustion characteristics of the ammonia/oxygen/nitrogen premixture.

2. Experimental setup and methods

2.1 Experimental apparatus

The schematic of the experimental setup is outlined in Fig. 1. The ammonia combustion experiments were carried out by using a constant-volume spherical chamber with a diameter of 200 mm and a height of 280 mm. The chamber's total volume was 6.19 $\times 10^{-3}$ m^3.

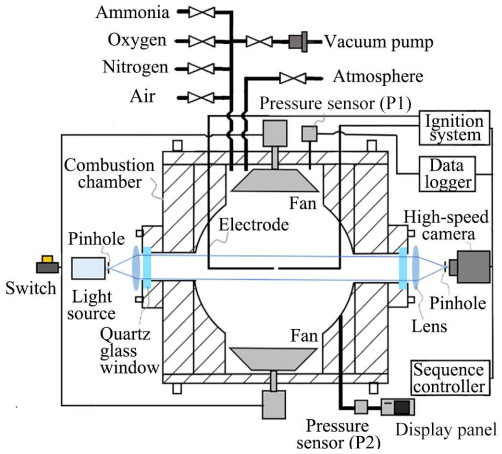

Fig. 1 Schematic of experimental apparatus.

A spark ignitor composed of two 2.0-mm-diam stainless-steel electrodes was employed in present research. The gap between the two electrodes' sharp tips was set to 2 mm. A capacitor discharge ignition (CDI) circuit system was connected to the spark electrode assembly to ignite the mixture. A series of capacitors with a total capacitance of 50 μF was charged by 469 volts direct current in the CDI circuit. The charged-voltage error was within ±1.5%. The electrostatic energy, charged in the capacitor circuit, was 5.5 J.

Turbulence was generated in the combustion chamber by two identical counter-rotation seven-bladed fans mounted vertically and symmetrically inside the chamber. Each fan was rotated by directly coupled electric motors (Maxon Motor, RE50) with separate speed controllers (Maxon Motor,

85 ESCON 50/5). The fans were precisely adjustable between 0 and 15,000 rpm. The fan rotation speed
86 error is within ± 1 rpm. Turbulence parameters were measured by particle image velocimetry (PIV)
87 measurement, as detailed in previous research [23]. In the center of the vessel that corresponds to the
88 region of optical access, the turbulence was found to be isotropic and homogeneous without regular
89 bulk motion. Turbulence intensity, u', was proportional to the fan speed [24], found to be represented
90 by Eq. (1):

91 $$u' = 0.00129 f_s \text{ m/s}, \quad (1)$$

92 where f_s is the fan speed in rpm. The longitudinal integral length scale, L_f, determined by two-
93 point correlation, was determined to be 20.9 mm regardless of the turbulence intensity [23].
94 Four optical-quartz glass observation windows were installed opposite each other in the chamber.
95 Flame propagation behavior was observed and recorded by schlieren photography, while the pressure
96 increase inside the chamber during flame propagation was measured with a pressure sensor (Valcom,
97 VPRTF-A4-(-0.1–2MPa) S-5, P1) and recorded by pressure transducer (GRAPHTEC, GL900) at 10
98 μs intervals. Schlieren photography was taken by a high-speed camera (Phantom, Miro C210) with
99 an LED light source (Hayashi-repic co., ltd., LA-HDF5010C). A pinhole was fixed in front of the
100 light source to form the spotlight effect. The pixel resolution of the camera was set to 576 × 576 with
101 a frame rate of 3000 fps.
102
103 **2.2 Experimental methods**
104 The experimental conditions are summarized in Table 1. In all the experiments, the initial pressure

and temperature were 0.1 MPa and 298 K. The temperature variations of the mixtures were within ±3 K. The turbulence intensity varied as 0–1.29 m/s. The composition of ammonia/oxygen/nitrogen mixture was defined by the equivalence ratio, ϕ, varied as 0.6–1.6, and was calculated on the basis of the ratio of ammonia to oxygen in the gas mixture [25] by Eq. (2):

$$\phi = \frac{(O/F)_{stoic}}{O/F} = \frac{F/O}{(F/O)_{stoic}}, \tag{2}$$

where F represents mole of ammonia, and O represents mole of oxygen in the premixed gas mixture.

Table 1
Experimental conditions of ammonia/oxygen/nitrogen premixture combustion

Experiment type	Ω	Equivalence ratio, ϕ	Turbulence intensity, u' (m/s)
Laminar	0.35	0.6, 0.8, 0.9, 1.0, 1.1, 1.2, 1.4	-
	0.4	0.6, 0.8, 0.9, 1.0, 1.1, 1.2, 1.4, 1.6	
Turbulent	0.4		0.32, 0.65, 0.97, 1.29

The chemical equation for ammonia/oxygen/nitrogen combustion under stoichiometric condition is given by Eq. (3):

$$NH_3 + 0.75/\Omega\,(\Omega\,O_2 + (1\text{-}\Omega)\,N_2) \rightarrow 0.25/\Omega\,(3\text{-}\Omega)\,N_2 + 1.5\,H_2O. \tag{3}$$

Ω is expressed by Eq. (4):

$$\Omega = \frac{X_{O_2}}{X_{O_2}+X_{N_2}}, \tag{4}$$

where X represents mole fraction. Taking consideration of the power density of ammonia flame and minimizing buoyancy effects [16,23,26], oxidizers with Ω of 0.35 and 0.4 were used for the research.

122 Laminar experiments under Ω = 0.35 were performed to verify the setup suitable for O_2-enriched
123 ammonia combustion experiments through comparing with the results of Mei et al. [16]. Experiments
124 on turbulent condition were carried out under $\Omega = 0.4$. The premixed gases had composition ratios
125 based on their partial pressures, as measured with a pressure sensor (Valcom, VPRTF-A4-(-0.1–
126 1MPa)-5, P2). The maximum errors of NH_3 concentration, O_2 concentration, and pressure inside the
127 chamber were 1.5%, 1.5%, 5%, respectively. After filling the ammonia/oxygen/nitrogen mixtures in
128 the chamber, an isotropic mixture was formed by running the top and bottom fans. In laminar
129 experiments, the mixtures were ignited after 5 minutes of finishing stirring. For turbulence
130 experiments, two fans were kept running during experiments. At least six experiments were
131 performed for each condition to ensure repeatability of the results.
132 Figure 2 shows the pressure history inside the combustion chamber for $\phi = 0.6$ and $\phi = 1.0$ at
133 $u' = 1.23$ m/s. The observation time range differed depending on the equivalence ratio and turbulence
134 intensity. For $\phi = 0.6$, the pressure was constant at ±5 % of ambient pressure during the observation
135 range (0–15 ms), whereas for $\phi = 1.0$, the observation range was lower because of the greater flame
136 propagation velocity. Overall, there was no pressure rise in the chamber during the observation range
137 for all conditions.

138

139

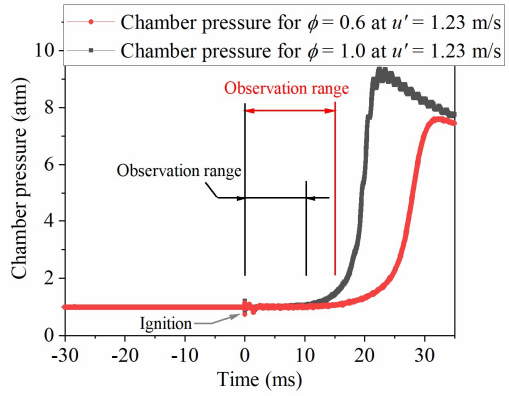

Fig. 2 Pressure history in chamber during combustion for ϕ = 0.6 and 1.0 at u' = 1.23 m/s.

3. Evaluation of burning velocity and ammonia/oxygen/nitrogen mixture properties

3.1 Evaluation of unstretched laminar burning velocity

Unstretched laminar burning velocity was derived from measuring the spherical propagation flame images obtained by the high-speed camera. The flame propagation velocity, S_n, was calculated from the mean flame radius, r_{sch}, of a circle whose area was equal to area of the schlieren image of spherical flame against time by Eq. (5):

$$S_n = \frac{dr_{sch}}{dt}. \tag{5}$$

During the laminar flame propagation process, the effects of the flame stretch must be considered, given that the spherically propagating flame had curvature. The flame stretch rate, ε, acting on the flame is defined [26–28] as Eq. (6):

$$\varepsilon = \frac{1}{Area} \bullet \frac{d(Area)}{dt} = \frac{2}{r_{sch}} \bullet \frac{dr_{sch}}{dt}, \tag{6}$$

where *Area* was the area of the spherical propagation flame front. Owing to the effect of diffusional–thermal instability, for non-unity Lewis number cases, the flame temperature and the laminar flame

propagation velocity were different from those in the unstretched case. The difference between stretched laminar flame propagation velocity, S_n, and unstretched laminar flame propagation velocity, S_S, can be expressed as a proportional relationship between burned gas Markstein length, L_b, and stretched rate, ε, as expressed [29] by Eq. (7):

$$S_S\text{-}S_n = L_b \bullet \varepsilon. \tag{7}$$

By extrapolating the stretched laminar flame propagation velocity to an infinite flame radius, which is equivalent to setting the flame stretched rate to 0, the unstretched laminar flame propagation velocity can be obtained. The unstretched laminar burning velocity, U_L, was derived from Eq. (8):

$$U_L = \frac{\rho_b}{\rho_u} \bullet S_S. \tag{8}$$

The stretched laminar burning velocity, U_N, was calculated by Eq. (9):

$$U_N = \frac{\rho_b}{\rho_u} \bullet S_n, \tag{9}$$

where ρ_u and ρ_b are unburned mixture density and burned mixture density, respectively.

Kelly et al. [30] found that outwardly propagating spherical flames in a constant-volume chamber may exhibit nonlinear relationship between the stretched flame propagation velocity, S_n, and stretched rate, ε. To extrapolate the unstretched laminar propagation velocity and the burned gas Markstein length, they proposed the nonlinear relationship expressed by Eq. (10):

$$(\frac{S_n}{S_S})^2 \, ln \, (\frac{S_n}{S_S})^2 = -2 \frac{L_b \varepsilon}{S_S}. \tag{10}$$

The unstretched laminar flame propagation velocity, S_S, and the burned gas Markstein number, L_b,

171 can be measured from linear extrapolation of ln(S_n) with ε/S_n^2 [14,31]. Okafor et al. [14] concluded
172 that the nonlinear equation was also appropriate for mixtures with Lewis numbers close to unity. In
173 our research, both linear and nonlinear equations were used to obtain the unstretched laminar burning
174 velocity, U_L, and the burned gas Markstein length, L_b.
175
176 **3.2 Evaluation of turbulent burning velocity**
177 The turbulent burning velocity is expressed by Eq. (11), the same as for the laminar burning
178 velocity [27,32,33]:

179 $$U_{tr} = \frac{\rho_b}{\rho_u} \bullet \frac{dr_{sch}}{dt}. \quad (11)$$

180 In the case of turbulent flames, the flame is deformed by turbulent eddies. Because the schlieren
181 image is integrated along the light path, it is impossible to define the three-dimensionally wrinkled
182 flame front by using the schlieren photography. However, Bradly and Kitagawa et al. [32] revealed
183 that such burning velocity could be correlated to the turbulent burning velocity by planer Mie-
184 scattered imagery, and they also came to an important conclusion that the turbulent burning velocity
185 was associated with the entrainment and mass-consumption rate of the unburned mixture.
186
187 **3.3 Ammonia/oxygen/nitrogen mixture properties**
188 Among the properties of the ammonia/oxygen/nitrogen mixtures (Table 2), ρ_b and ρ_u were
189 burned and unburned gas mixture densities were obtained from the Chemical Equilibrium Application
190 (CEA) computer program of the U.S. National Aeronautics and Space Administration [34]. λ, c_p, α,

191 v and Le were thermal conductivity, specific heat at constant pressure, thermal diffusivity,
192 kinematic viscosity, and the Lewis number which were calculated using the website of the Dandy
193 research group at Colorado State University [35]. The Lewis number is defined [36] by Eq. (12):

194 $$Le_i = \frac{\alpha}{D_{i/N_2}}, \tag{12}$$

195 where D_{i/N_2} is the mass diffusivity of the deficient species "i".

196 The effective Lewis number, Le_{eff}, of a single component fuel and an oxidizer can be expressed [37]
197 by Eq. (13):
198
199 $$Le_{eff} = 1 + \frac{(Le_E - 1) + (Le_D - 1)A}{1 + A}. \tag{13}$$
200
201 In this equation, the Lewis number Le_E and Le_D are those defined based on the reactant that is
202 relatively in excess and deficient, respectively. A represent a measure of the mixture's strength which
203 can be calculated by Eq. (14):

204 $$A = 1 + Ze(\Phi - 1). \tag{14}$$

205 The constant Φ, which is always >1, is defined as the mass ratio of excess-to-deficient reactants
206 in the mixture relative to their stoichiometric ratio [37,38]. Ze is Zel'dovich number which can be
207 expressed by Eq. (15):
208
209 $$Ze = E_a(T_{ad} - T_u)/(R^0 T_{ad}^2), \tag{15}$$
210
211 where R_0 is the universal gas constant, E_a is the activation energy which can be calculated [28,39] by

Eq. (16):

$$\frac{E_a}{R_0} = -2\frac{\partial \ln(\rho_u U_L)}{\partial (1/T_{ad})}. \quad (16)$$

As shown in Table 2, although the equivalence ratio changes greatly from 0.6 to 1.6 under oxygen content of 0.4, values of the effective Lewis number which change from 0.936 to 1.084, are very close to unity. Thus, the differential diffusion effect (characterized by the effective Lewis number) is comparably small.

Table 2
Properties of ammonia/oxygen/nitrogen mixtures [=, can't be defined]

Ω	ϕ	ρ_u [kg/m^3]	ρ_b [kg/m^3]	λ [10^{-3}W/m/K]	c_p [J/kg/K]	α [10^{-5}m^2/s]	v [10^{-5}m^2/s]	Le	T_{ad} [K]	Le_{eff}
0.35	0.6	1.0908	0.14938	27.559	1144.6	2.2074	1.560	0.896	2062.14	0.942
	0.8	1.0650	0.12707	27.804	1204.4	2.2034	1.556	0.894	2324.47	0.948
	0.9	1.0527	0.11985	27.911	1204.4	2.2012	1.554	0.883	2412.55	0.965
	1.0	1.0410	0.11483	28.015	1224	2.1987	1.552	=	2460.04	1.000
	1.1	1.0304	0.11249	28.099	1241.5	2.1966	1.550	1.125	2444.05	1.034
	1.2	1.0198	0.11227	28.181	1259.4	2.1943	1.549	1.122	2377.48	1.052
	1.4	1.0002	0.11419	28.337	1294.3	2.1889	1.545	1.119	2293.83	1.070
0.4	0.6	1.0861	0.13940	27.666	1155.2	2.2051	1.559	0.906	2182.39	0.936
	0.8	1.0570	0.11972	27.922	1200.7	2.2002	1.554	0.88	2423.05	0.945
	0.9	1.0440	0.11340	28.030	1221.8	2.1975	1.552	0.868	2497.35	0.963
	1.0	1.0319	0.10893	28.128	1241.9	2.1948	1.550	=	2534.38	0.999
	1.1	1.0206	0.10646	28.216	1261.1	2.1921	1.548	1.138	2521.72	1.033
	1.2	1.0101	0.10575	28.296	1279.5	2.1895	1.546	1.135	2463.98	1.052
	1.4	0.9909	0.107	28.435	1313.8	2.1842	1.543	1.13	2296.3	1.072
	1.6	0.97397	0.10978	28.552	1345.3	2.1791	1.5396	1.125	2122.21	1.084

4. Results and discussion

4.1 Flame observation

Figure 3 shows the sequence of schlieren images of ammonia/oxygen/nitrogen flames from 1 to 6

ms for $\phi = 0.6$ under laminar and four different turbulence intensity cases. It is apparent that as the turbulent flame expands outwardly, the flame becomes more wrinkled and accelerated. In the initial period of turbulent flame propagation, only eddies of a size smaller than the flame size could wrinkle the flame front, but with the development of the flame radius, the flame can be affected by wider range of turbulence wavelength. Also, Kolmogorov and Taylor's length scales become smaller as the turbulence intensity increases. Therefore, as the turbulence intensity increases, more smaller patterns of flame front deformations can be seen in Fig. 3. Also, the nonuniformity of the wrinkling effects of eddies increases with increasing turbulence intensity [40,41]. Accordingly, the flame propagates faster with increasing turbulence intensity.

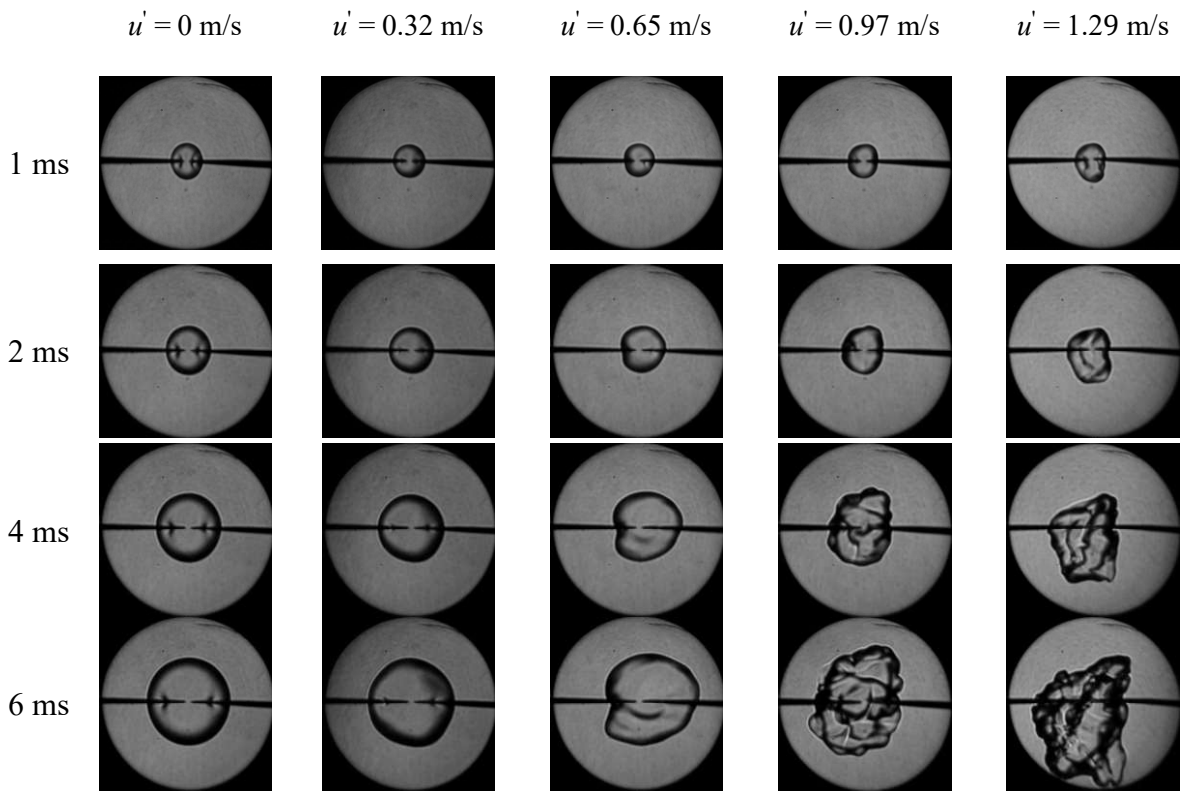

Fig. 3 Schlieren images of ammonia/oxygen/nitrogen mixtures under $\phi = 0.6$ at various turbulence intensities.

The 16-bit images were processed by gray levels from 0 = black (flame) to 255 = white

237 (background). The threshold value was selected based on visual inspection. The range of the threshold
238 value used for processing the images was from 50 to 100 depending on the obtained images. The
239 threshold-value effect on the radius and velocity deviations was within ±2% (see Appendix). Then
240 the processed image was transferred to the binary image in which the flame was black and background
241 was white. Subsequently, the flame area was calculated by the number of included pixels of the flame
242 area and the mean flame radius, r_{sch}, was determined by the radius of the equivalent circle area under
243 both laminar and turbulent conditions.

244 Figure 4 illustrates the flame radius as a function of elapsed time under $\phi = 0.6$ for various
245 turbulence intensities. It is apparent that at the beginning, the flame propagation was affected by the
246 ignition energy, but after the flame developed beyond the ignition affected period, under the same
247 elapsed time, the flame radius increased with the increase of turbulence intensity.

248

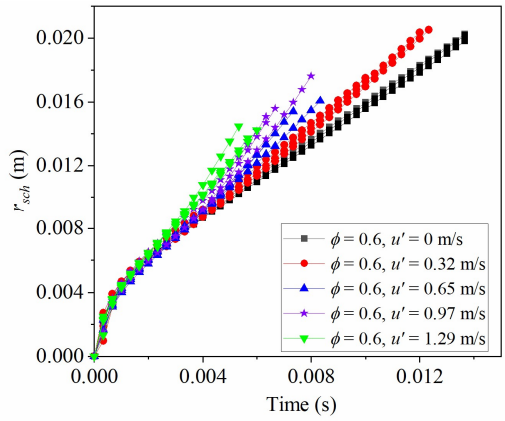

Fig. 4 Flame radius as function of time under $\phi = 0.6$ at various turbulence intensities.

249

250 **4.2 Unstretched laminar burning velocity of the ammonia/oxygen/nitrogen flame**

251 The ignition energy effect is checked by changing ignition energy from 0.3 to 5.5 J, as shown in

252 Fig. 5. The critical flame radius, which was used to eliminate the ignition energy affected period,
253 observed by ammonia/oxygen/nitrogen combustion for $\phi = 1.0$ at $\Omega = 0.4$, was ~0.008 m. (This
254 method was used by Chen et al.[42] and Huang et al. [43].) So, the radius that was < 0.008 m was not
255 counted in laminar and turbulent studies.
256

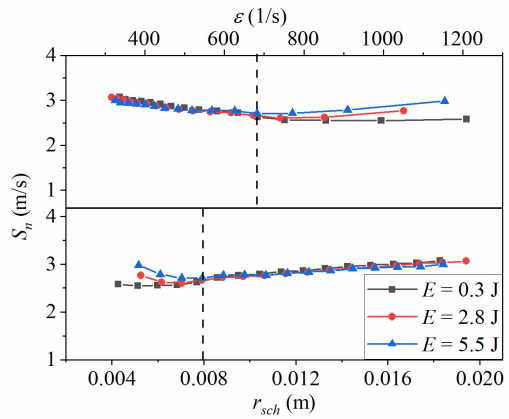

Fig. 5 Stretched laminar flame propagation velocity as functions of flame radius and stretch rate for ammonia/oxygen/nitrogen mixture at $\phi = 1.0$ on $\Omega = 0.4$.

257 In our research, the outwardly propagating spherical flame (OPF) in the constant-pressure method
258 was used to obtain the unstretched laminar burning velocity. Chen et al. [44] had noted that the
259 ignition energy, confinement, buoyancy, flame instability, and nonlinearity of the flame speed-stretch
260 rate relationship can cause inaccuracy of unstretched laminar flame speed measurement. The relation
261 between the stretched laminar flame propagation velocity, S_n, and the flame stretch rate, ε, under
262 conditions of $\phi = 0.8$ and $\phi = 1.2$ are shown in Fig. 6. According to Kelley [30], flame propagation
263 in a constant-pressure environment can be divided into three distinctive periods: an ignition energy
264 affected period, a quasi-steady period, and a chamber confinement affected period. The ignition
265 energy effected period was determined by the critical radius (Fig. 5). The confinement effect was
266 neglected because the observation period was relatively small compared with chamber volume. Mei

et al. [16] pointed out that the buoyancy effect on the ammonia/oxygen/nitrogen flame was almost eliminated under oxygen contents of 35% and 45% because flames for both were nearly spherical. The same phenomenon was found in present research. Also, the buoyancy effect was ignored because there was no noticeable change in the flame symmetry under any tested conditions. Too, because the flames within the observation range in the present study were stable, there was no uncertainty caused by instability. Additionally, linear and nonlinear methods were carefully applied to avoid the uncertainties induced by the nonlinearity of the flame speed-stretch rate relationship.

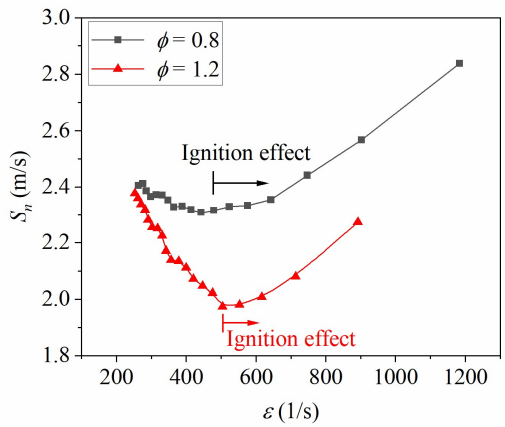

Fig. 6 The unstretched laminar propagation velocity as a function of stretch rate

Figure 7 shows the unstretched laminar burning velocities of the ammonia/oxygen/nitrogen premixture flame, which were obtained by using Eqs. (7) and (10). The results obtained by Mei et al. [16] by the same experimental method for $\Omega = 0.35$ were similar to those from our current research. Accordingly, the reproducibility of the flame propagation experiments of ammonia O_2-enriched combustion was confirmed.

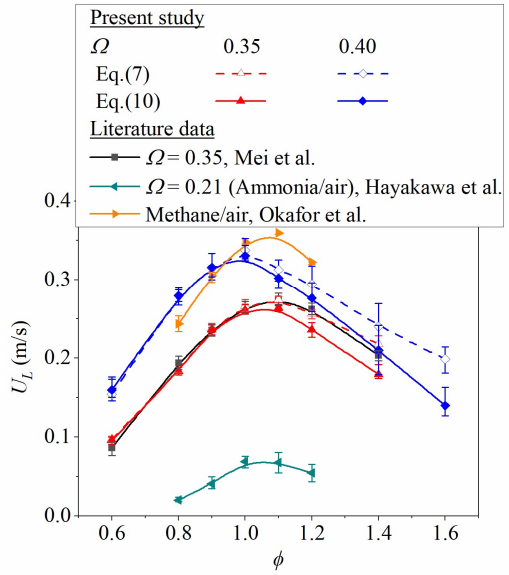

Fig. 7 Experimental results of correlation of unstretched laminar burning velocity with equivalence ratio under various oxygen contents in oxidizer

As indicated in Fig. 7, under the same ammonia/oxygen/nitrogen equivalence ratio, the unstretched laminar burning velocity of the ammonia/oxygen/nitrogen mixture increases with increasing Ω from 0.21 to 0.4. The maximum laminar burning velocity was 0.337 m/s at $\phi = 1.0$ under $\Omega = 0.4$ which was approximately 4.9 times the value under the condition $\Omega = 0.21$. From comparing with laminar burning velocity of CH_4/air [2], 40% oxygen content was found to enhance the ammonia laminar burning velocity to the level of methane/air laminar burning velocity.

On the other hand, the unstretched laminar burning velocities obtained from linear and nonlinear equations are approximately same on ammonia-lean and under stoichiometric conditions. However, the disparity increased with the rise of the equivalence ratio in ammonia-rich cases. The disparity between the two methods was considered by Okafor et al. [14] to have been caused by the increasing sensitivity of the flame to stretch.

The sensitivity of the laminar burning velocity to the flame stretch rate can be evaluated by the

294 burned gas Markstein length, L_b. Fig. 8 shows the burned gas Markstein length which was obtained

295 by the non-linear equation. Additionally, L_b increases with increase of ammonia equivalence ratio for

296 both Ω =0.35 and 0.4 cases.

297

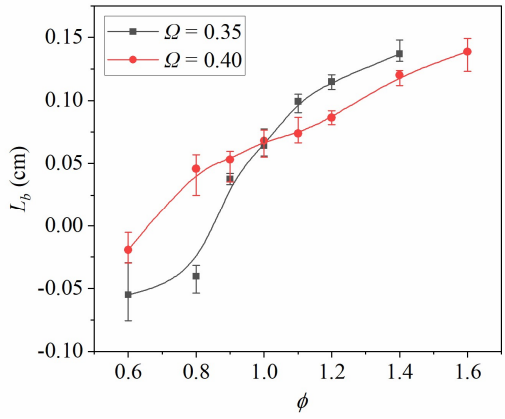

Fig. 8 Variation of the burned gas Markstein length with the equivalence ratio and oxygen content

298

299 From the asymptotic analysis of the premixed flame structure, L_b can be expressed [14,29] by Eq.

300 (17):

301

302 $$L_b = \delta_F[f_1(\sigma)+Ze(Le-1)f_2(\sigma)], \quad (17)$$

303

304 where the $f_1(\sigma)$ and $f_2(\sigma)$ are functions of the thermal-expansion coefficient and are always

305 positive for realistic coefficient values of σ [14]. In present research, the burned gas Markstein

306 length was dominated by the Zel'dovich number, flame thickness, and Lewis number. Flame

307 thickness, δ_F, is calculate [45] by Eq. (18):

308 $$\delta_F = \frac{\lambda}{c_p \rho_u U_L}. \quad (18)$$

309 Figure 9 shows the *Ze* and δ_F under different cases. Because *Ze* promotes the effect of a non-unity

310 Lewis number, the effect of an increase in *Ze* on the sensitivity of the flames to stretch depends on

311 the value of the Lewis number [14]. In ammonia-lean cases in which Le < 1, *Ze* decreases with

312 increasing L_b, while *Ze* increases with increasing L_b in ammonia-rich cases.

313

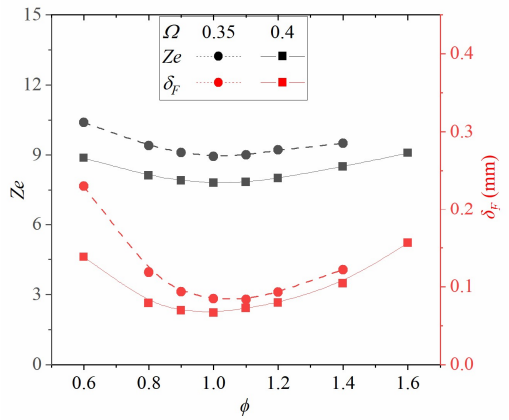

Fig. 9 Flame thickness and Zel'dovich number under different equivalence ratios and oxygen contents.

314 **4.3 Turbulent flame structure of ammonia/oxygen/nitrogen mixture under conditions of oxygen**

315 **enrichment**

316 To reveal the turbulence longitudinal integral length scale effect on the flame front, Borghi and

317 Peters proposed four kinds of turbulent flame regimes [19]. As shown in Fig. 10, the Peters regime

318 diagram indicates four flame regimes determined by the ratio of longitudinal integral length scale (L_f)

319 to laminar flame thickness (δ_F), with the ratio of turbulence intensity (u') to unstretched laminar

320 burning velocity (U_L), including the wrinkled flamelets regime, the corrugated flamelets regime, the

321 thin reaction zone, and the broken reaction zone.

322

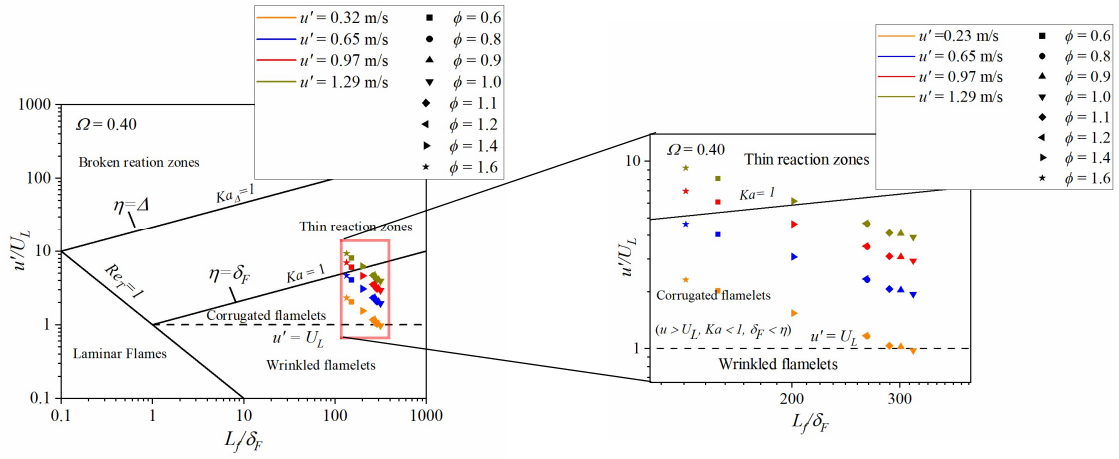

(a) Peters regime diagram

(b) Peters regime diagram in red square area

Fig. 10 Regimes of present experimental conditions on turbulent combustion diagram.

Most of the ammonia/oxygen/nitrogen turbulent flames were in the corrugated flamelets regime. In this regime, turbulent eddies push the flame front and undergo convolution, which increases the flame surface area (Fig.3) and the chemical reaction time is faster than the turbulent mixing. This means that the turbulent eddies can only wrinkle the laminar flamelets and cannot influence the chemical reaction within the flame front.

The turbulence Karlovitz number, which is the ratio of the chemical time scale to the time scale of turbulent eddies, can be calculated by Eq. (19) as a specific value of flame stretch caused by turbulent flow to turbulent flame [46]:

$$Ka = \frac{\delta_F}{U_L} \Big/ \frac{\lambda_f}{u'}, \tag{19}$$

where U_L is the unstretched laminar burning velocity, λ_f is the longitudinal Taylor microscale of turbulent field, and u' is turbulence intensity, δ_F is the thickness of preheat zone.

As shown in Fig. 11, the turbulent Karlovitz number (Ka) increases with increasing turbulence

intensity irrespective of the equivalence ratio. Moreover, it decreases with increasing equivalence ratio in ammonia-lean cases but it increases with increasing equivalence ratio in ammonia-rich cases. However, all $Ka < 1$. Thus, compared to the time scale of small eddies, chemical reaction rates were faster enough that turbulence eddies just wrinkled the flamelets and did not affect the chemical reaction within the flame front.

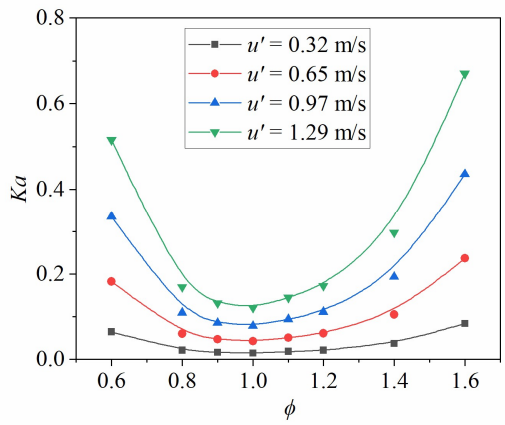

Fig. 11 Turbulence Karlovitz number (Ka) under different equivalence ratios and turbulence intensities.

4.4 Turbulence burning velocity of ammonia/oxygen/nitrogen mixture under condition of oxygen enrichment

Figure 12 shows the turbulent burning velocity U_{tr} and stretched laminar burning velocity U_N as functions of flame radius, r_{sch}, under various turbulence intensities at $\phi = 0.6$. As the flame radius increased from 0.004 m to 0.008 m, the turbulent burning velocity decreased because of the ignition energy effect. The ignition energy affected period, in which $r_{sch} < 0.008$ m, was ignored, but after the ignition energy affected period, the turbulent burning velocity increased with increasing flame radius for all turbulence intensity cases. For the same flame radius, the turbulent burning velocity increases with increasing turbulence intensity. The turbulent trends are the same for the other equivalence ratio cases.

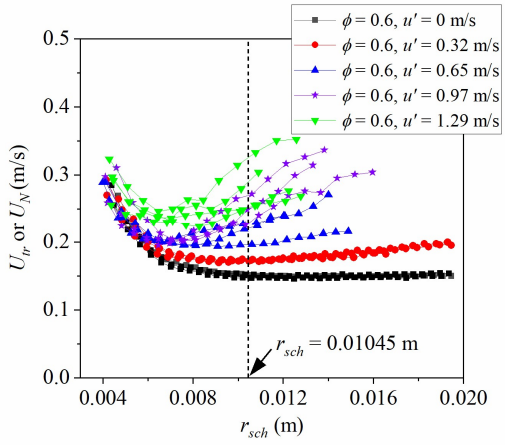

Fig. 12 Turbulent burning velocity developing as a function of flame radius for $\phi = 0.6$.

To examine the turbulence intensity effect on burning velocity, the burning velocity at flame diameter of the turbulence longitudinal integral length scale was used for comparison. The method has been used for studying premixed turbulent combustion of methane/air, hydrogen/methane/air, hydrogen/octane/air, hydrogen/air, iso-octane/air, methanol/air [24,47–52]. Moreover, for the laminar case, the stretched laminar burning velocity at flame diameter of the longitudinal integral length scale was used for comparison.

Figure 13 shows the turbulent burning velocity and stretched laminar burning velocity at flame diameter of L_f under various equivalence ratio, ϕ. It was found that turbulent burning velocity increases with increasing turbulence intensity. The increase of turbulent burning velocity of the ammonia/oxygen/nitrogen mixture is caused by the increase of the turbulent flame surface area deformed by turbulent eddies. Maximum turbulent burning velocity is at $\phi = 1.0$, the same as for unstretched laminar burning velocity. However, as shown in Fig. 13, somewhat large scatter is observed under conditions of high turbulence intensity. One reason for the large scatter is that the

367 flame is highly deformed at relative high turbulence intensities. This phenomenon has also been
368 observed in other instances of gaseous fuel turbulent flame propagation [53,54]. A second reason for
369 the scatter is that the effects of eddies on flame propagation increase with increasing turbulence
370 intensity. There are turbulent eddies of various sizes in the turbulent flow field, and the wrinkling
371 effects differ according to each eddy size [24]. Accordingly, the nonuniformity of wrinkling effects
372 of eddies increases with increasing turbulence intensity.
373

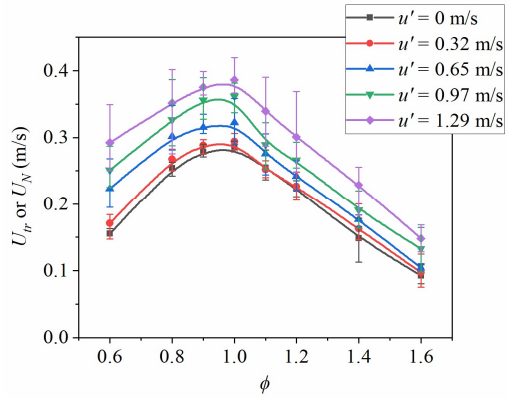

Fig. 13 Turbulent burning velocity and stretched laminar burning velocity at flame diameter of longitudinal integral length scale as a function of equivalence ratio.

374 Figure 14 shows the ratio of turbulent burning velocity to the stretched laminar burning velocity,
375 U_{tr}/U_N, as a function of ϕ. Through using the ratio U_{tr}/U_N, the effect of the global stretch that appears
376 in both the laminar and turbulent cases can be eliminated. Globally, the ratio U_{tr}/U_N decreases with
377 increasing equivalence ratio for ammonia-lean cases but increases with increasing of equivalence
378 ratio for ammonia-rich cases. Also, with increasing turbulence intensity, the ratio U_{tr}/U_N increases.
379 To examine these tendencies, the turbulence Karlovitz number, Ka, was introduced and the
380 relationship between turbulence Karlovitz number and the ratio of turbulent burning velocity to

stretched laminar burning velocity was studied.

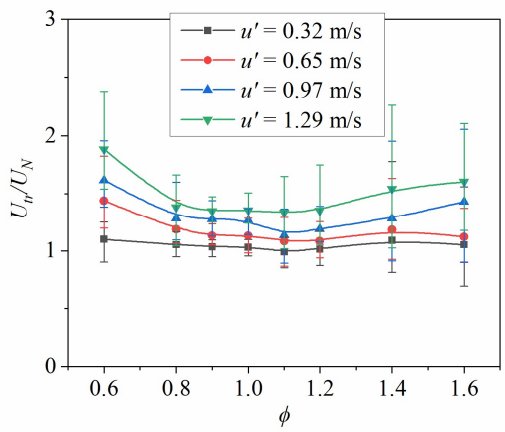

Fig. 14 The relation of the ratio of U_{tr}/U_N with ammonia equivalence ratio.

Figure 15(a) shows the relationship between turbulence *Ka* and U_{tr}/U_N. The ratio, U_{tr}/U_N, increases with increasing turbulence *Ka*. As shown in Fig. 15(b), the ratio U_{tr}/U_N for ammonia-lean cases, is higher than for ammonia-rich cases. This is most likely due to the effect of diffusional–thermal instability. The local burning velocity in the convex structure increases when $Le < 1$, i.e., the mass diffusion of reactants from the unburned area to the burned area excels the thermal diffusion from the burned area to the unburned area, and a convex structure develops. On the other hand, the local temperature and burning velocity in concave areas decrease, and a concave shape develops also. Eventually, overall burning velocity increases due to the increase in flame surface area because of the diffusional–thermal instability effect caused when $Le < 1$. Hence, turbulence eddies and the diffusional–thermal instability effect induced higher turbulent burning velocity in ammonia-lean cases under the same turbulence *Ka*. These findings indicate that not only the consideration of the turbulence effect but also the consideration of the diffusional–thermal instability effect is important

to predict the turbulent burning velocity of ammonia flame. Consideration of the effect of the diffusional–thermal instability when simulating flame propagation velocity can contribute greatly to the future design of combustor using ammonia as a fuel.

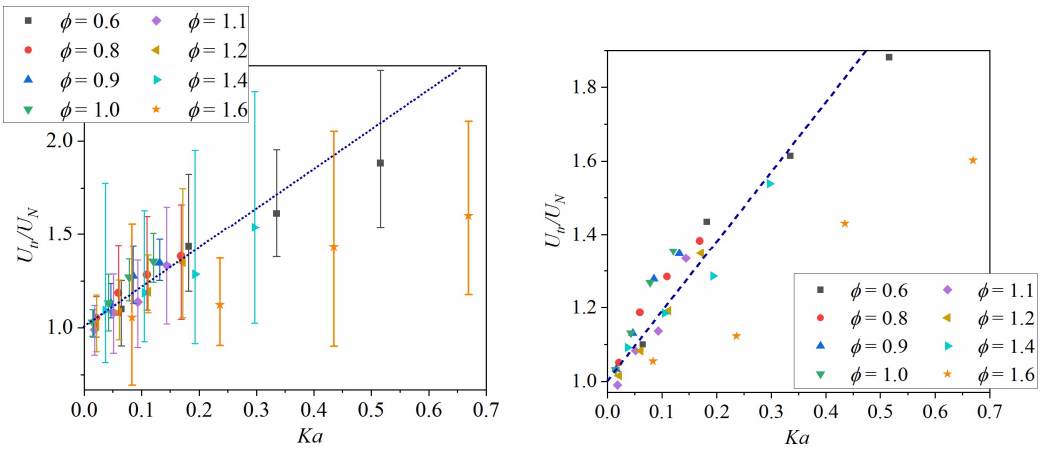

(a) U_{tr}/U_N as Ka under ϕ of 0.6–1.4 (b) U_{tr}/U_N as Ka under ϕ (without error bar)

Fig. 15 Ratio of turbulent burning velocity to stretched laminar burning velocity (U_{tr}/U_N) in terms of turbulence Karlovitz number (Ka).

However, for the case of $\phi = 0.6$, the U_{tr}/U_N as the turbulence Ka is slightly lower than the average line. This is considered to be caused by the lower adiabatic flame temperature, T_{ad}, which is shown in Table 2. For the case when $\phi = 1.6$, the Lewis number is almost the same as when $\phi = 1.4$. However, because of lower T_{ad}, the ratio of U_{tr}/U_N under the condition of $\phi = 1.6$ is much smaller than that in the case when $\phi = 1.4$. Hence, under the condition of $\phi = 0.6$, the lower adiabatic flame temperature limits the effect of diffusional–thermal instability. There is a possibility that the local quenching happens owing to the lower adiabatic flame temperature even though the basic diffusional–thermal instability effect is strong for ammonia-lean flame. That is, the contribution of the effect of diffusional-thermal instability to increase flame surface area is limited by local quenching due to the

lower adiabatic flame temperature for the case when ϕ = 0.6. Although the diffusional-thermal instability effect is limited for the ϕ = 0.6 case, it is still important because the ratio of U_{tr}/U_N under ϕ = 0.6 is much larger than that under ϕ = 1.6 even though T_{ad} is almost the same.

5. Conclusion

The effect of turbulence intensity on the burning characteristics of an ammonia/oxygen/nitrogen mixture was investigated under conditions of oxygen enrichment. The principal findings are as follows:

1. The turbulent burning velocity of the ammonia/oxygen/nitrogen flame increased with the increasing turbulence intensity owing to the increase of flame surface area (due to the increase of turbulence intensity).

2. Under the same turbulence Karlovitz number, the ratio of turbulent burning velocity to the stretched laminar burning velocity in ammonia-lean cases was larger than that in ammonia-rich cases. This is caused by the effect of diffusional-thermal instability. Consideration of both effects of the diffusional-thermal instability and the turbulence is important for the prediction of turbulent flame propagation velocity in ammonia combustion fields.

Acknowledgements

This work was partly supported by JSPS KAKENHI Grant Number JP19180646 and by JST PRESTO (Grant No. JPMJPR 1542) and the Collaborative Research Project of the Institute of Fluid Science, Tohoku University. Yu Xia was funded by the Chinese Scholarship Council (Grant no. 201806420020).

References

[1] Astbury GR. A review of the properties and hazards of some alternative fuels. Process Saf Environ Prot 2008;86:397–414. https://doi.org/10.1016/j.psep.2008.05.001.

[2] Li J, Huang H, Kobayashi N, He Z, Osaka Y, Zeng T. Numerical study on effect of oxygen content in combustion air on ammonia combustion. Energy 2015;93:2053–68. https://doi.org/10.1016/j.energy.2015.10.060.

[3] Joo JM, Lee S, Kwon OC. Effects of ammonia substitution on combustion stability limits and NO_x emissions of premixed hydrogen–air flames. Int J Hydrogen Energy 2012;37:6933–41. https://doi.org/10.1016/j.ijhydene.2012.01.059.

[4] Rui L, David.S.-K. T, M.David C. Ammonia as a fuel for SI engine. SAE Technical Paper 2003-01-3095. https://doi.org/10.4271/2003-01-3095.

[5] Lee JH, Lee SI, Kwon OC. Effects of ammonia substitution on hydrogen/air flame propagation and emissions. Int J Hydrogen Energy 2010;35:11332–41. https://doi.org/10.1016/j.ijhydene.2010.07.104.

[6] Michalsky R, Parman BJ, Amanor-Boadu V, Pfromm PH. Solar thermochemical production of ammonia from water, air and sunlight: Thermodynamic and economic analyses. Energy 2012;42:251–60. https://doi.org/10.1016/j.energy.2012.03.062.

[7] Kobayashi H, Hayakawa A, Somarathne KDKA, Okafor EC. Science and technology of ammonia combustion. Proc Combust Inst 2019;37:109–33. https://doi.org/10.1016/j.proci.2018.09.029.

[8] Grannell SM, Assanis DN, Bohac S V, Gillespie DE. The fuel mix limits and efficiency of a stoichiometric, ammonia, and gasoline dual fueled spark ignition engine. J Eng Gas Turbines Power 2008;130. https://doi.org/10.1115/1.2898837.

[9] Ronney PD. Effect of chemistry and transport properties on near-limit flames at microgravity. Combust Sci Technol 1988;59:123–41. https://doi.org/10.1080/00102208808947092.

[10] Ichikawa A, Hayakawa A, Kitagawa Y, Somarathne KDKA, Kudo T, Kobayashi H. Laminar burning velocity and Markstein length of ammonia/hydrogen/air premixed flames at elevated pressures. Int J Hydrogen Energy 2015;40:9570–8.

http://dx.doi.org/10.1016/j.ijhydene.2015.04.024.

[11] Li J, Huang H, Kobayashi N, He Z, Nagai Y. Study on using hydrogen and ammonia as fuels: Combustion characteristics and NO_x formation. Int J Energy Res 2014;38:1214–1223. https://doi.org/ 10.1002/er.3141.

[12] Kumar P, Meyer TR. Experimental and modeling study of chemical-kinetics mechanisms for H_2–NH_3–air mixtures in laminar premixed jet flames. Fuel 2013;108:166–76. https://doi.org/10.1016/j.fuel.2012.06.103.

[13] Henshaw PF, D' Andrea T, Mann KRC, Ting DS-K. Premixed ammonia-methane-air combustion. Combust Sci Technol 2005;177:2151–70. https://doi.org/10.1080/00102200500240695.

[14] Okafor EC, Naito Y, Colson S, Ichikawa A, Kudo T, Hayakawa A, et al. Experimental and numerical study of the laminar burning velocity of CH_4–NH_3–air premixed flames. Combust Flame 2018;187:185–98. https://doi.org/10.1016/j.combustflame.2017.09.002.

[15] Takeishi H, Hayashi J, Kono S, Arita W, Iino K, Akamatsu F. Characteristics of ammonia/N_2/O_2 laminar flame in oxygen-enriched air condition. Trans JSME (in Japanese) 2015;81:14–423. https://doi.org/10.1299/transjsme.14-00423.

[16] Mei B, Zhang X, Ma S, Cui M, Guo H, Cao Z, et al. Experimental and kinetic modeling investigation on the laminar flame propagation of ammonia under oxygen enrichment and elevated pressure conditions. Combust Flame 2019;210:236–46. https://doi.org/10.1016/j.combustflame.2019.08.033.

[17] Law CK. Combustion Physics. Cambridge: Cambridge University Press; 2006, p. 456-461. https://doi.org/10.1017/cbo9780511754517.

[18] Cuenot B. Gas Turbines and Engine Simulations, Adv Chem Eng. 2016;49:273–385. https://doi.org/10.1016/bs.ache.2016.09.004.

[19] Peters N. Turbulent Combustion. Cambridge: Cambridge University Press; 2001, p. 79. https://doi.org/10.1088/0957-0233/12/11/708.

[20] Hayakawa A, Arakawa Y, Mimoto R, Somarathne KDKA, Kudo T, Kobayashi H. Experimental investigation of stabilization and emission characteristics of ammonia/air premixed flames in a swirl combustor. Int J Hydrogen Energy 2017;42:14010–8. https://doi.org/10.1016/j.ijhydene.2017.01.046.

[21] Somarathne KDKA, Hatakeyama S, Hayakawa A, Kobayashi H. Numerical study of a low emission gas turbine like combustor for turbulent ammonia/air premixed swirl flames with a secondary air injection at high pressure. Int J Hydrogen Energy 2017;42:27388–99. https://doi.org/10.1016/j.ijhydene.2017.09.089.

[22] Somarathne KDKA, Hayakawa A, Kobayashi H. Numerical investigation on the combustion characteristics of turbulent premixed ammonia/air flames stabilized by a swirl burner. J Fluid Sci Technol 2016;11:jfst0026–jfst0026. https://doi.org/10.1299/jfst.2016jfst0026.

[23] Ichimura R, Hadi K, Hashimoto N, Hayakawa A, Kobayashi H, Fujita O. Extinction limits of an ammonia/air flame propagating in a turbulent field. Fuel 2019;246:178–86. https://doi.org/10.1016/j.fuel.2019.02.110.

[24] Hadi K, Ichimura R, Hashimoto N, Fujita O. Spherical turbulent flame propagation of pulverized coal particle clouds in an O_2/N_2 atmosphere. Proc Combust Inst 2019;37:2935–42. https://doi.org/10.1016/j.proci.2018.09.021.

[25] Stephen TR. An introduction to combustion concepts and applications. The McGraw-Hill Companies; 2012, p. 21-22. http://dx.doi.org/10.2139/ssrn.2257783.

[26] Hayakawa A, Goto T, Mimoto R, Arakawa Y, Kudo T, Kobayashi H. Laminar burning velocity and Markstein length of ammonia/air premixed flames at various pressures. Fuel 2015;159:98–106. http://dx.doi.org/10.1016/j.fuel.2015.06.070.

[27] Hayakawa A, Miki Y, Nagano Y, Kitagawa T. Analysis of turbulent burning velocity of spherically propagating premixed flame with effective turbulence intensity. J Therm Sci Technol 2012;7:507–21. https://doi.org/10.1299/jtst.7.507.

[28] Bradley D, Hicks RA, Lawes M, Sheppard CGW, Woolley R. The measurement of laminar burning velocities and markstein numbers for iso-octane–air and iso-octane–n-heptane–air mixtures at elevated temperatures and pressures in an explosion bomb. Combust Flame 1998;115:126–44. https://doi.org/10.1016/s0010-2180(97)00349-0.

[29] Clavin P. Dynamic behavior of premixed flame fronts in laminar and turbulent flows. Prog Energy Combust Sci 1985;11:1–59. https://doi.org/10.1016/0360-1285(85)90012-7.

[30] Kelley AP, Law CK. Nonlinear effects in the extraction of laminar flame speeds from expanding spherical flames. Combust Flame 2009;156:1844–51.

https://doi.org/10.1016/j.combustflame.2009.04.004.

[31] Chen Z. On the extraction of laminar flame speed and Markstein length from outwardly propagating spherical flames. Combust Flame 2011;158:291–300. https://doi.org/10.1016/j.combustflame.2010.09.001.

[32] Bradley D, Haq MZ, Hicks RA, Kitagawa T, Lawes M, Sheppard CGW, et al. Turbulent burning velocity, burned gas distribution, and associated flame surface definition. Combust Flame 2003;133:415–30. https://doi.org/10.1016/s0010-2180(03)00039-7.

[33] Okafor EC, Fukuda Y, Nagano Y, Kitagawa T. Turbulent burning velocities of stoichiometric hydrogen-carbon monoxide-air flames at elevated pressures. SAE Technical Papers 2014-01-2701. https://doi.org/10.4271/2014-01-2701.

[34] Gordon S, McBride B. Computer program for calculation of complex chemical equilibrium compositions and applications 1996:1311.

[35] Dandy D. Bioanalytical Microfluidics Program, Color State Univ n.D. (n.d.). http://navier.engr.colostate.edu/(accessed 13.08.19).

[36] Bouvet N, Halter F, Chauveau C, Yoon Y. On the effective Lewis number formulations for lean hydrogen/hydrocarbon/ air mixtures. Int J Hydrogen Energy 2013;38:5949–60. https://doi.org/10.1016/j.ijhydene.2013.02.098.

[37] Addabbo R, Bechtold JK, Matalon M. Wrinkling of spherically expanding flames. Proc Combust Inst 2002;29:1527–35. https://doi.org/10.1016/s1540-7489(02)80187-0.

[38] Okafor EC, Nagano Y, Kitagawa T. Experimental and theoretical analysis of cellular instability in lean H_2-CH_4-air flames at elevated pressures. Int J Hydrogen Energy 2016;41:6581–92. https://doi.org/10.1016/j.ijhydene.2016.02.151.

[39] Jomaas G, Law CK, Bechtold JK. On transition to cellularity in expanding spherical flames. J Fluid Mech 2007;583:1–26. https://doi.org/10.1017/s0022112007005885.

[40] Brequigny P, Halter F, Mounaïm-Rousselle C. Lewis number and Markstein length effects on turbulent expanding flames in a spherical vessel. Exp Therm Fluid Sci 2016;73:33–41. https://doi.org/10.1016/j.expthermflusci.2015.08.021.

[41] Cai X, Wang J, Bian Z, Zhao H, Zhang M, Huang Z. Self-similar propagation and turbulent burning velocity of CH_4/H_2/air expanding flames: Effect of Lewis number. Combust Flame

544 2020;212:1–12. https://doi.org/10.1016/j.combustflame.2019.10.019.
545 [42] Chen Z, Burke MP, Ju Y. Effects of Lewis number and ignition energy on the determination of
546 laminar flame speed using propagating spherical flames. Proc Combust Inst 2009;32:1253–60.
547 https://doi.org/10.1016/j.proci.2008.05.060.
548 [43] Huang Z, Zhang Y, Zeng K, Liu B, Wang Q, Jiang D. Measurements of laminar burning
549 velocities for natural gas-hydrogen-air mixtures. Combust Flame 2006;146:302–11.
550 https://doi.org/10.1016/j.combustflame.2006.03.003.
551 [44] Chen Z. On the accuracy of laminar flame speeds measured from outwardly propagating
552 spherical flames: Methane/air at normal temperature and pressure. Combust Flame
553 2015;162:2442–53. https://doi.org/10.1016/j.combustflame.2015.02.012.
554 [45] Jarosinski J. The thickness of laminar flames. Combust Flame 1984;56:337–342.
555 https://doi.org/10.1016/0010-2180(84)90067-1.
556 [46] Kitagawa T, Nagano Y, Tsuneyoshi K. Study on the effects of pressure on turbulent burning
557 velocity of outwardly propagating propane-air flame with Turbulence Reynolds and Markstein
558 numbers. Nihon Kikai Gakkai Ronbunshu, B Hen/Transactions Japan Soc Mech Eng Part B
559 2006;72:825–32. https://doi.org/ 10.1299/kikaib.72.825.
560 [47] Kitagawa T, Nakahara T, Maruyama K, Kado K, Hayakawa A, Kobayashi S. Turbulent burning
561 velocity of hydrogen–air premixed propagating flames at elevated pressures. Int J Hydrogen
562 Energy 2008;33:5842–9. https://doi.org/10.1016/j.ijhydene.2008.06.013.
563 [48] Mandilas C, Ormsby MP, Sheppard CGW, Woolley R. Effects of hydrogen addition on laminar
564 and turbulent premixed methane and iso-octane–air flames. Proc Combust Inst 2007;31:1443–
565 50. https://doi.org/10.1016/j.proci.2006.07.157.
566 [49] Lawes M, Ormsby MP, Sheppard CGW, Woolley R. The turbulent burning velocity of iso-
567 octane/air mixtures. Combust Flame 2012;159:1949–59.
568 https://doi.org/10.1016/j.combustflame.2011.12.023.
569 [50] Fairweather M, Ormsby MP, Sheppard CGW, Woolley R. Turbulent burning rates of methane
570 and methane-hydrogen mixtures. Combust Flame 2009;156:780–90.
571 https://doi.org/10.1016/j.combustflame.2009.02.001.
572 [51] Lawes M, Ormsby MP, Sheppard CGW, Woolley R. Variation of turbulent burning rate of

methane, methanol, and iso-octane air mixtures with equivalence ratio at elevated pressure. Combust Sci Technol 2005;177:1273–89. https://doi.org/10.1080/00102200590950467.

[52] Vancoillie J, Sharpe G, Lawes M, Verhelst S. The turbulent burning velocity of methanol-air mixtures. Fuel 2014;130:76–91. https://doi.org/10.1016/j.fuel.2014.04.003.

[53] Bradley D, Haq MZ, Hicks RA, Kitagawa T, Lawes M, Sheppard CGW, et al. Turbulent burning velocity, burned gas distribution, and associated flame surface definition. Combust Flame 2003;133:415–30. https://doi.org/10.1016/s0010-2180(03)00039-7.

[54] Goulier J, Chaumeix N, Halter F, Meynet N, Bentaïb A. Experimental study of laminar and turbulent flame speed of a spherical flame in a fan-stirred closed vessel for hydrogen safety application. Nucl Eng Des 2017;312:214–27. https://doi.org/10.1016/j.nucengdes.2016.07.007.